Int. J. Radiation Oncology Biol. Phys., Vol. 50, No. 4, pp. 915–928, 2001

0360-3016/01/$–see front matter

PII S0360-3016(01)01548-6

CLINICAL INVESTIGATION **Brain**

MR-SPECTROSCOPY GUIDED TARGET DELINEATION FOR HIGH-GRADE GLIOMAS

ANDREA PIRZKALL, M.D.,*† TRACY R. MCKNIGHT, PH.D.,‡ EDWARD E. GRAVES, B.S.,‡ MARK P. CAROL, M.D.,† PENNY K. SNEED, M.D.,* WILLIAM W. WARA, M.D.,* SARAH J. NELSON, DR.RER.NAT.,‡ LYNN J. VERHEY, PH.D.,* AND DAVID A. LARSON, M.D., PH.D.*

*Department of Radiation Oncology, University of California, San Francisco, San Francisco, CA; †Department of Radiation Oncology, University of Heidelberg and German Cancer Research Center, Heidelberg, Germany; ‡Department of Radiology, Magnetic Resonance Science Center, University of California, San Francisco, San Francisco, CA

Purpose: Functional/metabolic information provided by MR-spectroscopy (MRSI) suggests MRI may not be a reliable indicator of active and microscopic disease in malignant brain tumors. We assessed the impact MRSI might have on the target volumes used for radiation therapy treatment planning for high-grade gliomas.

Methods and Materials: Thirty-four patients (22 Grade III; 12 Grade IV astrocytomas) were evaluated; each had undergone MRI and MRSI studies before surgery. MRI data sets were contoured for T1 region of contrast enhancement (T1), region of necrosis, and T2 region of hyperintensity (T2). The three-dimensional MRSI peak parameters for choline (Cho) and *N*-acetylaspartate (NAA), acquired by a multivoxel technique, were categorized based on an abnormality index (AI), a quantitative assessment of tissue metabolite levels. The AI data were aligned to the MRI and displayed as three-dimensional contours. AI vs. T conjoint and disjoint volumes were compared.

Results: For both grades, although T2 estimated the region at risk of microscopic disease as being as much as 50% greater than by MRSI, metabolically active tumor still extended outside the T2 region in 88% of patients by as many as 28 mm. In addition, T1 suggested a lesser volume and different location of active disease compared to MRSI.

Conclusion: The use of MRSI to define target volumes for RT treatment planning would increase, and change the location of, the volume receiving a boost dose as well as reduce the volume receiving a standard dose. Incorporation of MRSI into the treatment-planning process may have the potential to improve control while reducing complications. © 2001 Elsevier Science Inc.

Brain tumor, Astrocytoma, High-grade glioma, Magnetic resonance imaging (MRI), MR-spectroscopy (MRSI), Intensity-modulated radiation therapy (IMRT).

INTRODUCTION

The prognosis for patients diagnosed with Grade III or Grade IV astrocytoma remains dismal: median survival is 9–12 months, following a combination of surgery and standard external beam radiation therapy (RT) (1). As a result, there is continued interest in exploring novel means of treating these patients. Many of these, such as immunotherapy, radiosurgical boost RT, and image-guided surgery, target specific portions of the tumor identified on imaging studies. Especially within the field of RT, new delivery technologies, such as radiosurgery (RS) and intensity-modulated radiation therapy (IMRT), allow the creation of exquisitely conformal dose distributions that are able simultaneously to increase dose to certain portions of the tumor volume and spare normal tissue (2).

To garner the most benefit from these techniques, it is critical that the regions identified for special attention be defined accurately; areas of active tumor (suitable for high dose) must be identified separately (as gross tumor volume or GTV) from areas suspicious for tumor extension that are suitable for a lower dose (classified as clinical target volume

Reprint requests to: Dr. Andrea Pirzkall, Department of Radiation Oncology, University of California, San Francisco, 505 Parnassus Avenue, L-75, San Francisco, CA 94143-0226. E-mail: pirzkall@radonc17.ucsf.edu

Presented at the 42nd American Society for Therapeutic Radiology and Oncology (ASTRO) meeting, October 23rd, 2000, in Boston, MA; winning the Resident Clinical/Basic Research Award.

These studies were supported in part by the NIH through Grants RO1 CA79719 and T32 CA66527, and by the NOMOS Corporation, Sewickley, PA.

Acknowledgments—The authors would like to thank Dr. M. W. McDermott and Dr. M. W. Berger from the Department of Neurologic Surgery for referring their patients for this study, Dr. M. D. Prados and Dr. S. Chang from the Department of Neurologic Surgery, Neuro-Oncology Service for many helpful discussions, and M. A. Takahashi form the Magnetic Resonance Science Center for assistance in data analysis.

Accepted for publication 23 February 2001.

or CTV). The standard approach to defining target volumes in patients with high-grade gliomas is to deliver a certain dose to the contrast enhancing area, as determined from a contrast enhanced T1-weighted magnetic resonance imaging (MRI) or a computed tomography (CT) scan, plus a margin of 1–4 cm (1, 3–5). Some protocols deliver an additional dose to the contrast enhancing area itself; a lower dose may be delivered to the T2-weighted region of hyperintensity plus a variable margin (6, 7).

The gadolinium-enhancing lesion, as seen on T1-weighted MRI, reflects regions where there has been a breakdown of the blood–brain barrier. This may not be a reliable indicator of active tumor due to the presence of nonenhancing tumor tissue or contrast-enhancing necrosis. Therefore, information that can improve the definition of the spatial extent of tumor may improve the ability to define the volumes to which dose should be delivered.

One such source of information is three-dimensional (3D) multivoxel magnetic resonance-spectroscopy imaging (MRSI). This technique provides information about tumor activity based upon the levels of cellular metabolites, including choline (Cho), creatine (Cre), *N*-acetylaspartate (NAA), and lactate/lipid. Cho is a neurotransmitter and membrane component that is increased in tumors; Cre is indicative of cellular bioenergetic processes; NAA is a neuronal metabolite, not present in other central nervous system (CNS) cells, that is decreased in tumors; lactate is an end product of anaerobic metabolism whose presence can represent cellular breakdown; and lipid occupies the same resonant frequency as lactate.

A number of techniques have been developed for obtaining proton (^{1}H) spectra from selected regions within the brain (8–10). These techniques provide either a single spectrum or a multidimensional array of spectra from the region of interest. Studies over the past decade have suggested that an assessment of the degree of alteration in metabolite levels may help differentiate normal from abnormal tissue in patients suspected of harboring a high-grade glioma (HGG) (11–18). A consistent finding from these studies has been that gliomas exhibit a markedly high resonance in the spectral region of Cho and/or a low NAA resonance, implying an increase in the Cho to NAA ratio. A series of studies at our institution have examined the correlation between MRSI spectra and biopsy samples obtained under image guided targeting. The results demonstrate that the degree of elevation in Cho level correlates with an elevation in tumor cell density (19).

The effect the use of MRSI data might have on treatment planning has been explored by others. Graves *et al.* studied the prognostic value of MRSI in Gamma Knife radiosurgery of recurrent malignant gliomas (20). In a retrospective study, they demonstrated that those patients who had a MRI contrast enhancement determined treatment volume, with no MRSI suspected tumor pattern outside the contrast enhancement, had a significantly better outcome than those patients who had MRSI suspected disease that extended outside the MRI derived treatment volume. They concluded that pretreatment MRSI results provide information that may improve the selection, planning and treatment process for glioma patients. As a result, UCSF now uses MRSI on an active basis to define treatment volumes for Gamma Knife RS (21).

In this study, we investigated whether the use of metabolic data would affect the definition of target volumes for radiation therapy treatment planning for patients diagnosed with HGG.

METHODS AND MATERIALS

Thirty-four patients with HGG seen between February 1997 and July 2000 were selected for this study. Each patient had undergone an MRI and MRSI study before definitive surgery as part of an ongoing study conducted by one of the authors (TRM) examining the correlation between MRSI data and tumor grade as assessed by serial biopsies. Twenty-two patients had a pathologic diagnosis of astrocytoma World Health Organization (WHO) Grade III (15 anaplastic astrocytomas, 6 anaplastic oligoastrocytomas, 1 anaplastic oligodendroglioma), and 12 of astrocytoma WHO Grade IV (glioblastoma multiforme, GBM), by Word Health Organization II Criteria.

MRI

For each patient, MRI examinations were performed on a 1.5 Tesla GE Signa MR scanner (General Electric Medical Systems, Milwaukee, WI) using a quadrature head coil. MRI data sets included (*1*) an axial fluid-attenuated inversion recovery (FLAIR) sequence and/or a fast spin echo (FSE) sequence as T2-weighted sequences with 3-mm slice thickness, and (*2*) T1-weighted pre- and post-gadolinium contrast-enhanced spoiled gradient echo (SPGR) volume sequence with 1.5-mm slice thickness. The acquisition parameters used in these studies have been reported elsewhere (22).

^{1}H MR-spectroscopy

At the conclusion of the MRI study, a 3D chemical shift imaging (CSI) multivoxel MRSI sequence was prescribed. A point-resolved spectroscopy sequence (PRESS) was used for volume localization. Acquisition time constraints restricted the size of the region of interest from which MRSI data could be obtained. Typical acquisitions consisted of a $16 \times 8 \times 8$ cm or $12 \times 12 \times 8$ cm matrix ("PRESS-box") with a nominal spatial resolution of 1 cc (1 cc/voxel). To allow for the recording of control spectra, the PRESS-box volume was positioned so as to extend beyond the suspected disease to include normal brain from the contralateral hemisphere, even if this meant that the entire region of suspected disease could not be covered. It was also positioned to avoid areas of subcutaneous lipid and varying magnetic susceptibility that might compromise the quality of the spectra.

The raw spectral data were reconstructed using software developed at the UCSF Magnetic Resonance Science Center (22). The peak parameters (height, width, area) for Cho and NAA were estimated on a voxel-by-voxel basis within the

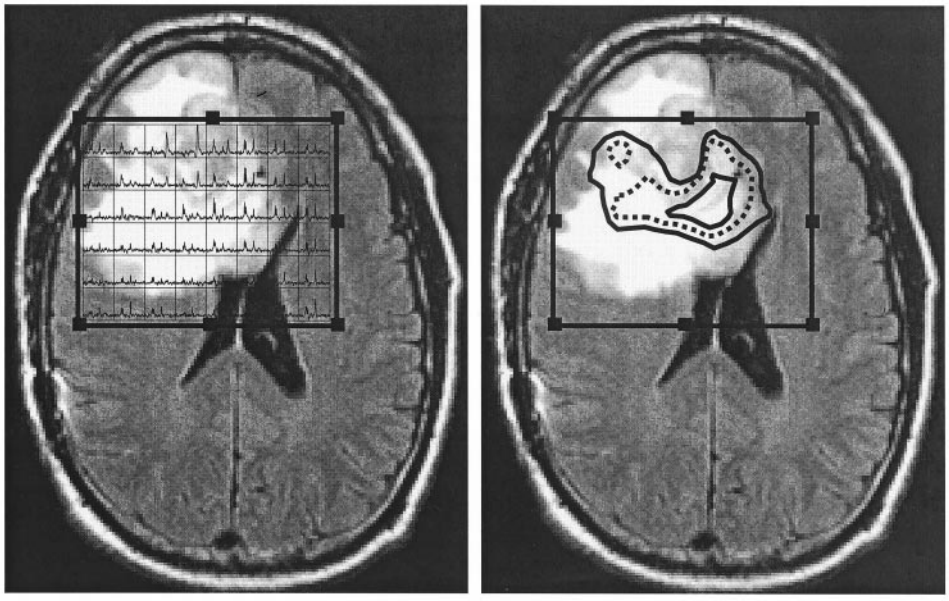

Fig. 1. Functional image: [1]H-MRSI with spectral signal and abnormality index (AI) contours within the defined PRESS-box (point-resolved spectroscopy sequence, PRESS). The outer and inner solid lines are the AI2 and AI4 contours, respectively, and the dotted line is the AI3 contour.

excited region (Fig. 1). A previously developed automated statistical analysis served to identify a control population of spectra acquired from normal tissue from the contralateral hemisphere included within the image volume from the studied patient (23). The degree of spectra abnormality, on a voxel-by-voxel basis, was determined by evaluating the number of standard deviations of difference between the relative Cho and NAA levels within a given voxel and that of the control voxels. This quantitative score was referred to as the abnormality index (AI) defined by its residual or z-score (23). Although there is technically no upper limit to AI levels, an ongoing study, correlating selected biopsy samples with AI values calculated for the exact sample location, has found an AI of 2 (95% confidence limit) to be

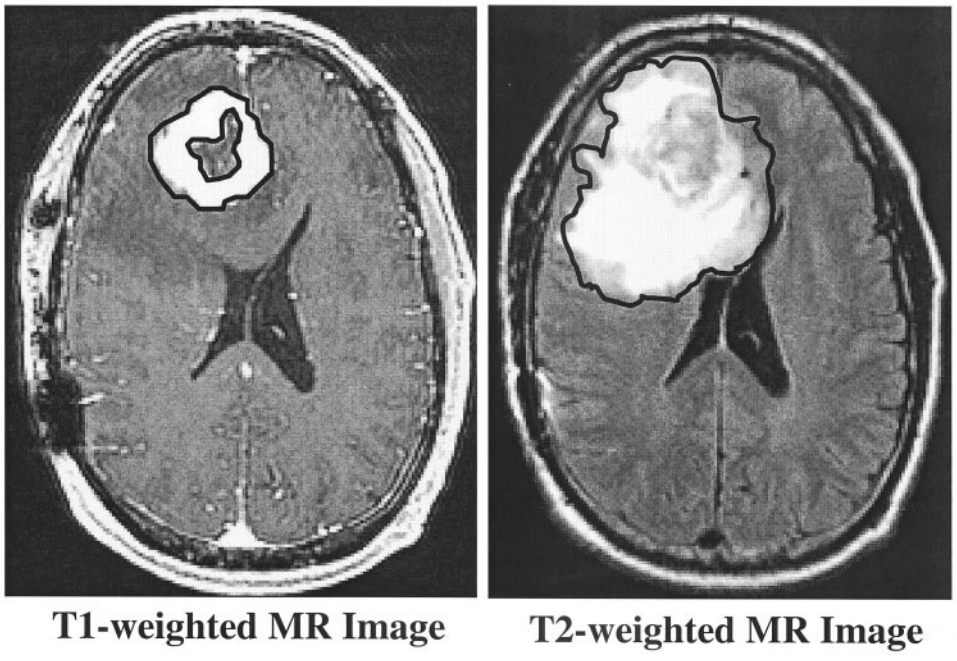

Fig. 2. Anatomic image: MRI with T1- and T2-weighted images showing the definition of T1, T2, and necrotic volumes in a patient with glioblastoma multiforme (GBM) imaged before surgery.

the lowest value corresponding to tumor (24). Because it is not clear what levels of metabolic activity should be considered as representing active disease, microscopic disease, GTV, CTV, and/or boost volumes, we defined and evaluated specifically AI levels of 2, 3, and 4. After automatic alignment to the MRI, these AI contours were displayed on the MRI as contour maps (Fig. 1).

MRI/MRSI volumetric evaluation

Each MRI data set was contoured manually by one of the authors (AP) (Fig. 2). Regions of interest included T1 contrast enhancement (T1) and T2 hyperintensity (T2). The T1 volume included the region of either solid or patchy enhancement without additional margin. Any hypointense centrally demarcated areas within the T1 contrast enhancement were defined as necrosis and segmented separately. The T2 volume was contoured as the area of hyperintensity on either FSE and/or FLAIR images. The ventricular system was removed by varying window and level.

These volumes were then compared to the MRSI AI contours using an interactive image analysis program developed at the Magnetic Resonance Science Center. This comparison was complicated by the fact that the PRESS-box did not always include the entire T1 and T2 volumes. Therefore, to allow for a representative comparison of the two techniques, the T1 and T2 volumes were reduced by the amount of T1 and T2 that were not covered by the PRESS-box, leaving the "T1-clipped" (T1c) and "T2-clipped" (T2c) volumes. In addition, because areas of necrosis, as assessed on MRSI, have a different but defined spectral signature, they were defined as distinct volumes by the statistical analysis program and, therefore, were not included in the AI volumes. As a result, the T1c volume was reduced further by subtracting the volume of necrosis, if any, that had been defined on the MR images.

Conjoint (overlapping) and disjoint (mutually exclusive) MRI and MRSI volumes were then compared. As a working hypothesis, we decided to designate and compare AI2 and T2c as measures of microscopic disease. Because it was not clear what AI level should be used to measure gross disease, we compared T1c vs. AI2, AI3, and AI4 as possible measures (Fig. 3). In addition, the maximum extension of the AI2 volume outside the T2c volume was measured to assess how far beyond the T2 volume metabolically determined microscopic disease could be detected. Similar measurements were made for AI2, AI3, and AI4 relative to the T1c volume for metabolically active disease. All maximum distances were measured perpendicular to the outer border of the volume of comparison.

RESULTS

The median age at time of diagnosis was 35 years for the 22 Grade III patients and 41 years for the 12 Grade IV patients. The total MR examination time was approximately 90 min, of which 17 min were used for MRSI acquisition.

MRI volumes

Fifteen of 22 Grade III and 11 of 12 Grade IV tumors were contrast enhancing at the time of examination. In 3 Grade III and 6 Grade IV tumors, areas of necrosis, defined as regions of solid hypointensity, were seen (0.6, 0.9, and 2.6 cc; and 2.3, 3.1, 3.8, 4.1, 8.6, and 10.7 cc, respectively).

FSE images were available for study in all but 2 patients, each of whom had undergone a FLAIR sequence only. Based upon the finding of only a 13% difference in the T2 volume, as derived from FSE vs. FLAIR sequences in the 5 patients in whom both had been acquired, it was decided that the FLAIR derived volumes could be used for these 2 patients for the purpose of this study.

MRI clipped volumes

The tumor volumes as demarcated by T1- and T2-weighted MR images are listed in Table 1 according to the percentage of their volumes that were evaluated by spectroscopy. The mean percentages of the T1 and T2 volumes included in the PRESS-box for Grade III and Grade IV were 83 and 87% for the T1, and 66% and 67% for the T2 evaluations.

MRI/MRSI volume comparisons

Grade III gliomas. Table 2 and Fig. 4 summarize the relationship between AI2 and T2c for Grade III patients. Thirteen of 22 (60%) patients had T2c volumes that were greater than the AI2 volume. The volume of AI2 on average was 78% of the volume of T2c, with 82% of AI2 encompassed by T2c.

AI2 disease extended ipsilaterally beyond T2c disease in 21/22 patients (Table 3). Although the extension was not uniform around the T2c volume, the maximum extension averaged 9 mm (range, 3–12 mm), and the volume extending beyond T2c was greater than 5 cc in 16/22 patients. In addition, 10 patients had metabolic activity (AI2) suggestive of tumor following white matter tracts to the contralateral hemisphere (8 patients) or along the optic radiation (2 patients). Only 2 of these patients had T2 disease indicating the same white matter tract extension. For the 8 patients who had AI2 white matter tract extension but not T2 extension, AI2 extended outside T2 by an average of 20 mm (median 20, range 12–28).

Table 4 and Fig. 5 summarize the relationships between AI2, AI3, and AI4 and T1c for Grade III patients. Of the 22 patients, 22, 21, and 18 (100%, 95%, 82%) had T1c volumes that were smaller than the AI2, AI3, and AI4 volumes, respectively. Seven patients did not have a T1c volume at all, i.e., there was no contrast enhancing lesion. In summary, at all AI levels, the AI volume was significantly larger than the T1c volume (552%, 329%, 196% for AI2, AI3, and AI4 relative to T1c, respectively), with the vast majority of the T1c volume being subsumed by the AI volume (92%, 82%, and 69% of T1c inside AI2, AI3, and AI4, respectively).

Ipsilateral AI volume extension beyond the T1c volume was substantial (Table 3). Although it was not uniform, for

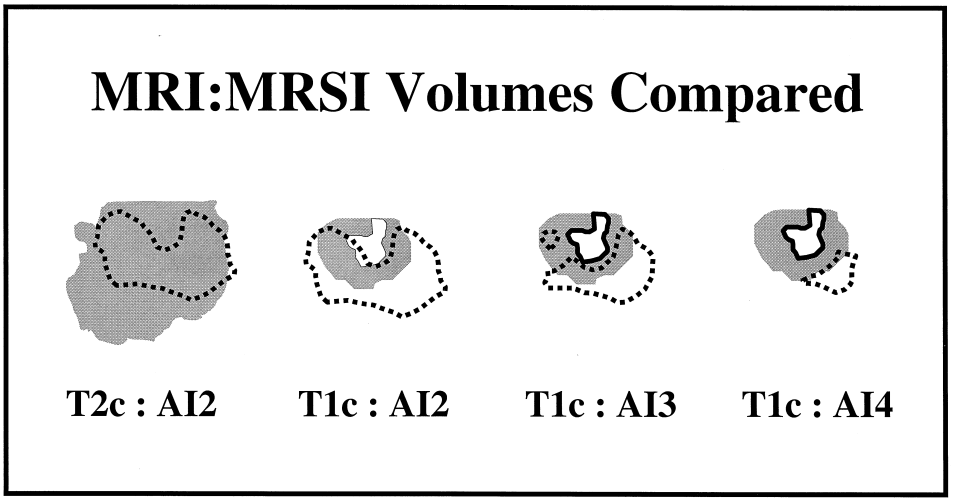

Fig. 3. Fused MRI/MRSI volumes in categories of interest. Dotted lines represent the abnormality index (AI) contours, shaded areas represent T volumes.

the 15/22 patients who had a T1c volume, the maximum AI2, AI3, and AI4 extension beyond the T1c margin averaged 30, 27, and 23 mm, respectively. In addition, 6 patients had AI2 but not T1c volumes following white matter tracts to the contralateral hemisphere. In these patients, AI2 extended outside T1c by an average of 38 mm (median 37, range 31–50).

Grade IV gliomas. Table 2 and Fig. 6 summarize the relationship between AI2 and T2c for Grade IV patients. Ten of 12 patients (83%) had T2c volumes that were greater than the AI2 volume. The volume of AI2 on average was 58% of the volume of T2c, with 83% of A2 encompassed by T2c.

The AI2 disease extended ipsilaterally beyond T2c disease in 9/12 patients (75%). Although the extension was not uniform around the T2c volume, maximum extension averaged 9 mm (range, 6–12 mm), and the volume extending beyond T2c was greater than 5 cc in 7 patients (Table 3). In addition, seven patients had metabolic activity (AI2) suggestive of tumor following white matter tracts to the contralateral hemisphere (5 patients) or along the optic radiation (2 patients). Similar tumor extension on T2 also was suggestive in 5 patients. For the 2 patients who had AI2 white matter tract extension but not T2 extension, AI2 extended outside T2 by 14 and 21 mm.

Table 5 and Fig. 7 display the relationships between AI2, AI3, and AI4 and T1c for Grade IV patients. For the 12 patients, 11, 7, and 5 (92%, 59%, and 42%) had T1c volumes that were smaller than the AI2, AI3, and AI4 volumes, respectively. Of these, 1 patient did not have a T1c contrast-enhancing volume. The variance in size between the T1c and the AI volumes was not as large as was seen in the Grade III patients: 213%, 117%, and 71% for AI2, AI3, and AI4 relative to T1c respectively. In addition, although much of the T1c volume was subsumed by the AI2 volume (mean 83%), the AI3 vs. T1c and AI4 vs. T1c volumes were quite disjoint, with approximately 50% of each lying outside the other.

Ipsilateral AI volume extension beyond T1c volume,

Table 1. MRI-derived T1 and T2 volumes with respect to the extent of the PRESS-box

Astrocytoma grade	Mean	Median	Range
Grade III (n = 22)			
T1 volume (cc)	17	9	2–77
T1c volume (cc)	15	8	1–64
% T1 covered by PRESS-box	83	94	14–100
T2 volume (cc)	113	99	24–231
T2c volume (cc)	72	60	17–141
% T2 covered by PRESS-box	67	67	48–83
Grade IV (n = 12)			
T1 volume (cc)	28	25	5–115
T1c volume (cc)	24	19	5–85
% T1 covered by PRESS-box	87	95	53–100
T2 volume (cc)	128	114	32–259
T2c volume (cc)	76	68	26–140
% T2 covered by PRESS-box	66	60	41–96

Table 2. Astrocytomas Grade III and Grade IV: Relationship of MRI T2c and MRSI AI2 volumes

Astrocytoma grade	Mean	Median	Range
Grade III (n = 22)			
T2c volume (cc)	72	60	17–141
AI2 volume (cc)	56	47	18–149
AI2 outside of T2c (cc)	11	6	0–48
% AI2 outside of T2c (%)	18	13	0–58
T2c outside of AI2 (cc)	27	23	3–83
% T2c outside of AI2 (%)	36	37	7–75
Grade IV (n = 12)			
T2c volume [cc]	76	68	26–140
AI2 volume [cc]	44	40	18–100
AI2 outside of T2c [cc]	8	8	0–32
% AI2 outside of T2c [%]	17	18	0–37
T2c outside of AI2 [cc]	48	45	3–104
% T2c outside of AI2 [%]	58	61	9–100

although not as great as was seen with Grade III patients, still was substantial (Table 3). Although it was not uniform, for the 11/12 patients who had a T1c volume, the maximum AI2, AI3, and AI4 extension beyond the T1c margin averaged 18, 14, and 10 mm, respectively. In addition, 5 patients had AI2 but not T1 volumes following white matter tracts to the contralateral hemisphere. In these patients, AI2 extended outside T1 by an average of 23 mm (median 24, range 16–28).

DISCUSSION

Despite a lack of consistent evidence for a strong dose–response curve beyond 60 Gy when using radiation to treat HGG, there continues to be great interest in employing higher doses (6, 7, 25). Early experience suggests an increase in local dose to ≥ 90 Gy using accelerated mixed proton/photon irradiation may improve freedom from progression (FFP) and survival in HGG (7). However, this

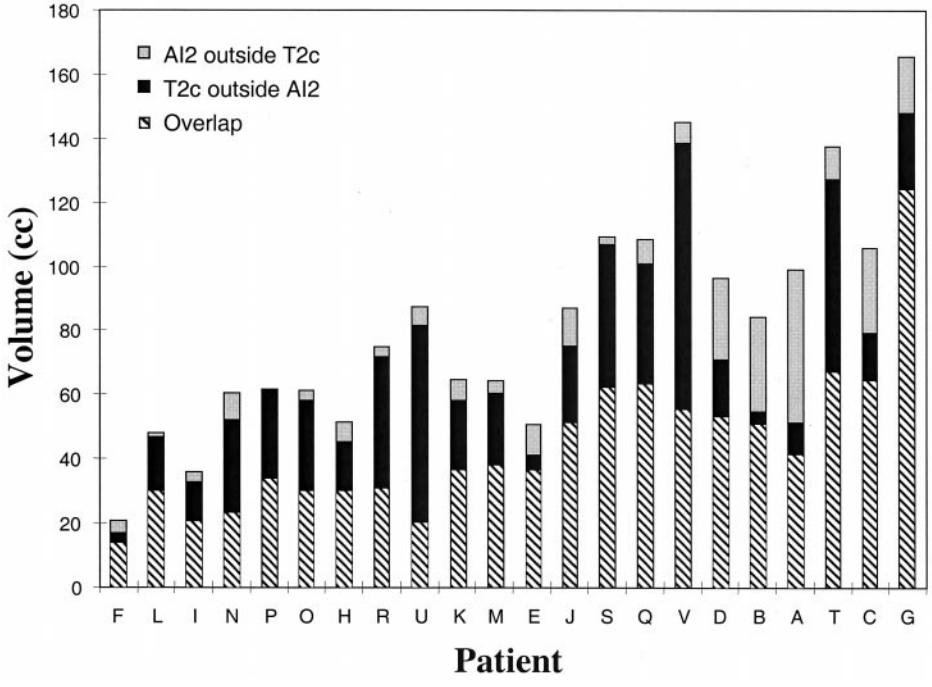

Fig. 4. Volumetric analysis for Grade III astrocytoma patients; disjoint and conjoint volumes for T2c and AI2.

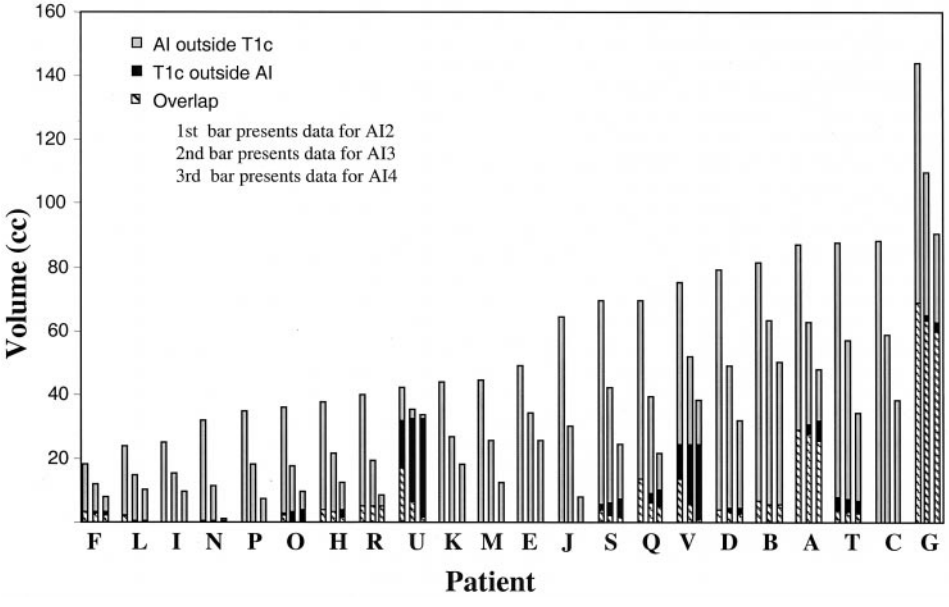

Fig. 5. Volumetric analysis for Grade III astrocytoma patients; disjoint and conjoint volumes for T1c and AI2, AI3, and AI4. Seven of the 22 tumors were not contrast enhancing.

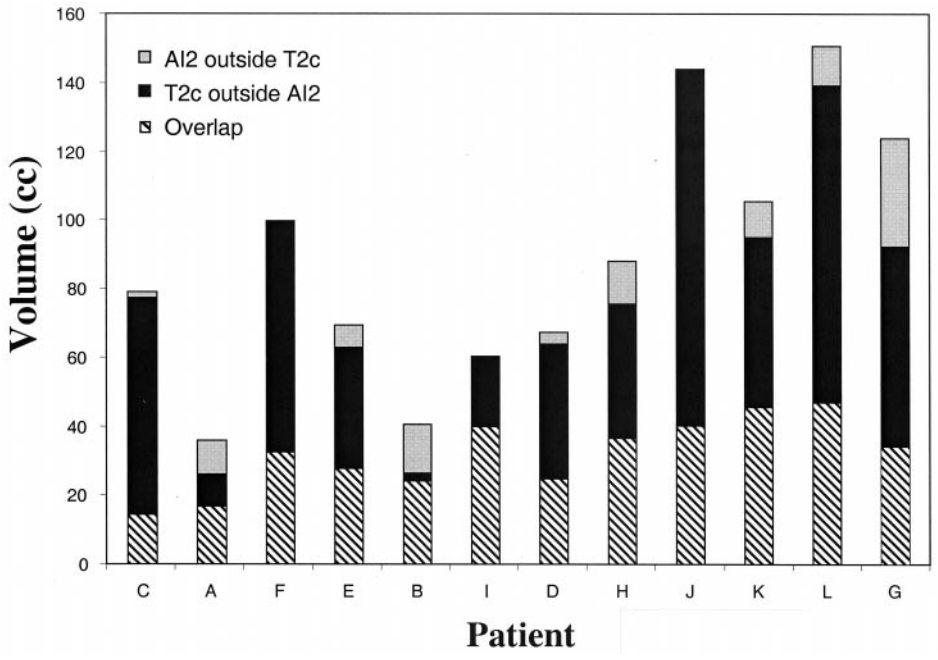

Fig. 6. Volumetric analysis for Grade IV astrocytoma patients; disjoint and conjoint volumes for T2c and AI2.

regimen also carries with it an increased incidence of side effects.

It can be postulated that the use of such high doses may be of greatest clinical value only if "all" of the active disease receives a certain dose and if normal tissue is spared as much as possible. Accurate target definition thus becomes of prime importance. MRI has become the imaging technique of choice for treatment planning for RT because it has been shown to be more sensitive than CT with regard to detection of tumor extension (26). The standard approach to defining target volumes in patients with HGG is to add a 1- to 4-cm margin to the contrast enhancing area, as determined from a T1-weighted MRI (1, 3–5). The size of this margin has been chosen based upon two traditional lines of reasoning: (*1*) serial biopsies of patients undergoing craniotomy for malignant gliomas reveal tumor cells more than 3 cm distant from the contrast enhancing margin (27, 28); (*2*) about 80% of relapses occur within a 2-cm margin from the original tumor location (5, 29, 30).

There are several problems with the standard approach.

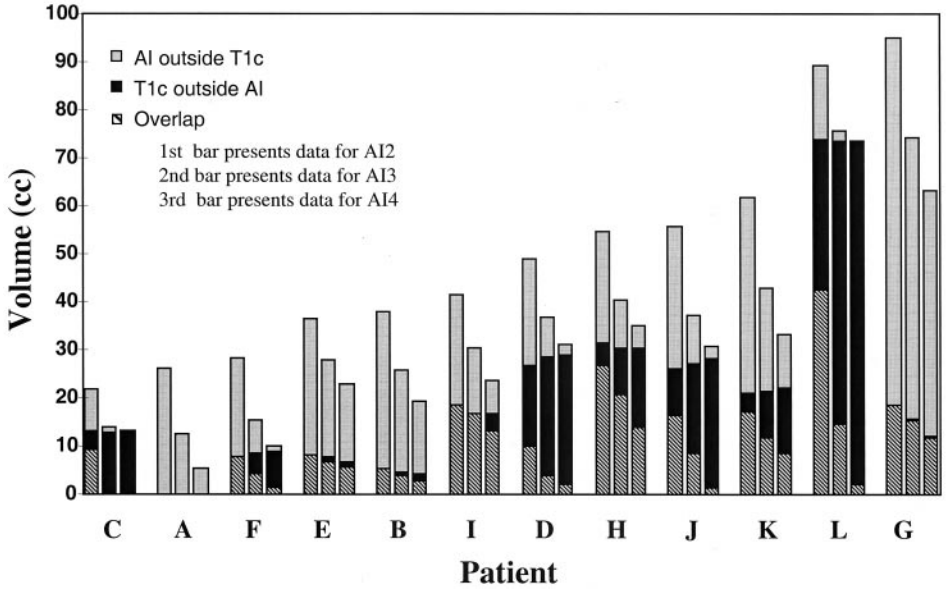

Fig. 7. Volumetric analysis for Grade IV astrocytoma patients; disjoint and conjoint volumes for T1c and AI2, AI3, and AI4. One of the 12 tumors was not contrast enhancing.

Table 3. Astrocytomas Grade III and Grade IV: MRSI detected ipsilateral tumor extension outside MRI volumes

Astrocytoma grade	Mean	Median	Range
Grade III ($n = 22$)			
AI2 outside of T1c (mm)	30	27	11–48
AI3 outside of T1c (mm)	27	24	9–45
AI4 outside of T1c (mm)	23	21	7–39
AI2 outside of T2c (mm)	9	9	3–12
Grade IV ($n = 12$)			
AI2 outside of T1c (mm)	18	18	9–27
AI3 outside of T1c (mm)	14	14	6–25
AI4 outside of T1c (mm)	10	11	5–24
AI2 outside of T2c (mm)	8	10	6–12

The gadolinium-enhancing lesion as seen on T1-weighted MRI may not always correspond to the region of active disease due to the presence of nonenhancing tumor tissue and to the presence of contrast enhancing necrosis. Nonspecific processes, such as inflammation or reactive edema formation, also may appear hyperintense on T2-weighted MRI, making it difficult to determine what is and what is not tumor. In addition, serial biopsy studies show tumor cells extending in a variable pattern beyond the enhancement region, in the area of edema, and even in normal appearing brain adjacent to the region of T2 abnormality (31). Serial biopsy studies have shown also that tumor infiltration tends to follow white matter fiber tracts (32).

The variability in tumor cell distribution makes it difficult to define an effective, yet safe, margin for purposes of treatment planning. A uniform margin can be expected to cover either too much noninfiltrated brain or to leave small areas of tumor infiltration out of the treatment volume. The latter is undesirable because it will increase the likelihood of local recurrence. The former is equally unacceptable because it is clear that radiation induced CNS toxicity is related not only to dose but to volume as well (33). Because focal RT appears to decrease neuropsychologic sequelae when compared to large volume RT (29, 34), and since the goal of any revised treatment protocol is to prolong survival, a margin that is tailored to tumor extension, rather than one that is uniform, could be presumed to improve quality of survival as well as local control.

We are not the first to suggest that alternative imaging modalities may have a role in delineating target volumes. Modalities under evaluation include positron emission tomography (PET) (35) and I-123-alpha-methyl-tyrosine SPECT (IMT-SPECT) (36). Studies by Mosskin *et al.* (37) and Ogawa *et al.* (38) have concluded that PET using methyl-11C-L-methionine (MET) better demonstrates the true extent of brain gliomas than CT or MRI but that it is of little value in defining tumor grade or in separating regions from necrosis. A recent study, reporting on the use of IMT-SPECT in 30 patients with nonresected, histologically proven brain gliomas (Grade II–IV astrocytomas and oligodendrogliomas), demonstrated IMT-SPECT activity incorporating partially or completely the MRI contrast enhancement volume with extension outside the region of

Table 4. Astrocytoma Grade III: Relationship of MRI contrast enhancing volume (T1c) and MRSI volumes (AI2, AI3, and AI4)

	T1c vol. (cc)	AI2 vol. (cc)	AI2/ T1c (%)	AI2 outside T1c (cc)	T1c outside AI2 (cc)	AI2 outside T1c (% AI2)	T1c outside AI2 (% T1c)	AI3 vol. (cc)	AI3/ T1c (%)	AI3 outside T1c (cc)	T1c outside AI3 (cc)	AI3 outside T1c (% AI3)	T1c outside AI3	AI4 vol. (cc)	AI4/ T1c (%)	AI4 outside T1c (cc)	AI4 outside T1c (% AI4)	T1c outside AI4 (cc)	T1c outside AI4 (% T1c)
Mean	10	56	552	48	2	89	8	33	329	28	3	89	18	20	196	15	88	4	31
Median	4	47	1063	47	0	97	0	28	641	27	0	99	1	13	303	12	99	1	19
Min.	0	18		10	0	38	0	10		3	0	32	0	0		0	32	0	0
Max.	64	149		88	15	100	48	109		59	25	100	78	87		44	100	31	100

enhancement in all patients studied (36). The IMT region of abnormality was 69% greater than the region of T1-weighted contrast enhancement, and 23% of patients had IMT uptake beyond the T2 hyperintensity by as much as 2 cm.

A more universally available modality is proton magnetic resonance spectroscopy (^{1}H-MRSI). It has been applied to patients with brain tumors since the late 1980s, demonstrating significant differences in spectra between tumor and normal brain tissue. The MRSI data can be obtained as part of a conventional MRI examination by suppressing the large signal from water protons and then monitoring the variation in intensity of protons from intracellular metabolites such as cholin, creatine and NAA.

Many of these studies applied a single-voxel technique to provide a single spectrum from a defined volume of tissue as large as $4 \times 4 \times 4$ cm (39–42). The lack of spatial resolution in such a technique prevents it from providing information on the spatial distribution of disease. Recent advances in MRI techniques, proposed as early as 1982 (43), allow the excitation and recording of a multidimensional array of spectra from hundreds of contiguous voxels each 1 cc or less in size (40, 44, 45). This increase in spatial resolution, and the associated decrease in partial volume effects, makes the 3D MRSI technique of potential value in target volume definition.

The spectral components that are of interest for evaluating brain tumors *in vivo* correspond to the peaks generated by choline containing compounds, Cre, lactate/lipid, and NAA. Cho appears to be an indicator of cell membrane biosynthesis; it can be decreased in cortical gray matter compared to subcortical white matter (46) and is increased in those conditions associated with cellular hyperplasia and neuronal degeneration, such as phospholipid metabolism and myelin degradation (23, 47, 48). NAA is predominantly present in neurons; a decrease in NAA could be caused by lower functional activity (49) or by a loss in neuronal cells or displacement by infiltrating tumor (15, 40, 50–52). There is a variation in the Cho and NAA ratio in normal brain, but this is considered small by most investigators when compared to the difference between normal and diseased brain.

A consistent finding among MRSI studies has been that gliomas exhibit a markedly high resonance in the spectral region of Cho and/or a low NAA resonance (19, 23), yielding an increase in the Cho to NAA ratio. A series of studies at our institution have addressed the correlation between MRSI spectra and biopsy samples obtained under image guided targeting. Dowling *et al.* have shown that the degree of elevation in Cho level correlates with an elevation in tumor cell density (19). When Cho levels are two standard deviations above, and NAA levels two standard deviations below, normal levels, 100% of pathohistologic specimens demonstrate tumor. Even when Cho is less than two standard deviations elevated compared to normal but is greater than NAA, the histology is tumor in 85% of specimens. In

Table 5. Astrocytoma Grade IV: Relationship of MRI contrast enhancing volume (T1c) and MRSI volumes (AI2, AI3, and AI4)

	T1c vol. (cc)	AI2 vol. (cc)	AI2/ T1c (%)	AI2 outside T1c (cc)	AI2 outside T1c (% AI2)	T1c outside AI2 (cc)	T1c outside AI2 (% T1c)	AI3 vol. (cc)	AI3/ T1c (%)	AI3 outside T1c (cc)	AI3 outside T1c (% AI3)	T1c outside AI3 (cc)	T1c outside AI3 (% T1c)	AI4 vol. (cc)	AI4/ T1c (%)	AI4 outside T1c (cc)	AI4 outside T1c (% AI4)	T1c outside AI4 (cc)	T1c outside AI4 (% T1c)
Mean	21	44	213	29	67	5	17	24	117	15	65	12	45	15	71	10	52	15	54
Median	16	40	253	25	73	0	7	22	136	11	67	7	41	11	70	5	52	10	56
Min.	0	18		9	25	0	0	1		1	12	0	0	0		0	0	0	0
Max.	72	100		77	100	32	58	76		59	100	59	98	61		51	100	72	100

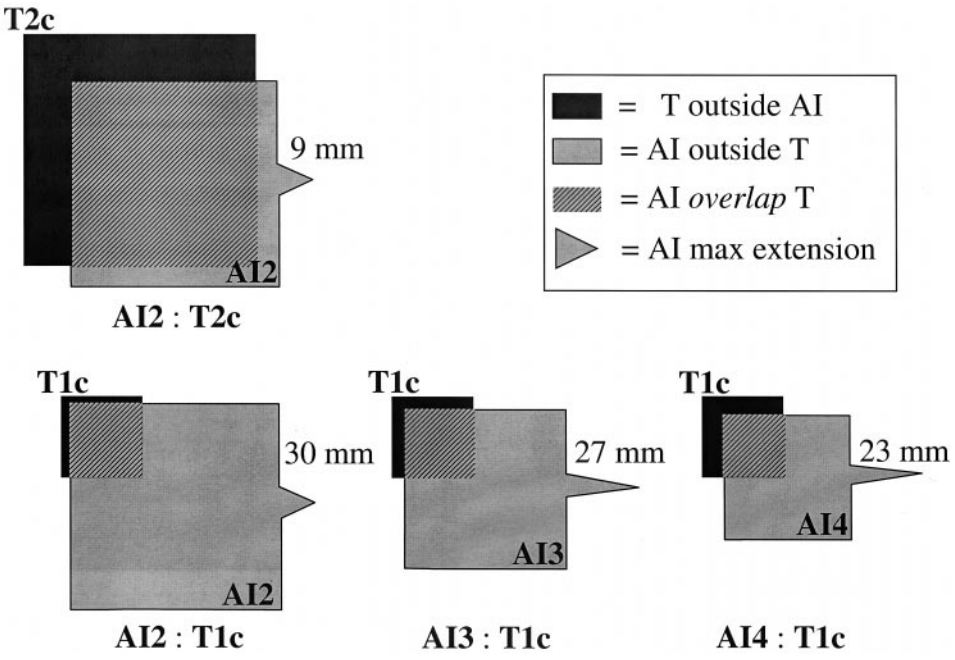

Fig. 8. Graphic summary of results for Grade III astrocytoma patients. The average relative sizes of the total volumes, the conjoint and disjoint volumes, and the maximum extension of the abnormality index (AI) volume beyond the T volume are displayed.

addition, an ongoing study by one of the authors (TRM) has shown that an AI of ≥ 2 is diagnostic in 98% of samples for the presence of tumor (97 biopsy samples in 42 patients) (24).

This study found that the volumes targeted for treatment, based on anatomic and metabolic imaging, would be of different sizes and located in different areas (Figs. 8 and 9), depending on whether they were generated based on MRI or MRSI. In general, the MRI suggests a larger volume of microscopic disease, as defined by T2 hyperintensity. However, despite the fact that most of the MRSI determined AI2 volume was contained within the MRI derived T2c volume, 95% of Grade III and 75% of Grade IV tumors still had AI2 extensions outside of the T2c volume that averaged 9 and 8

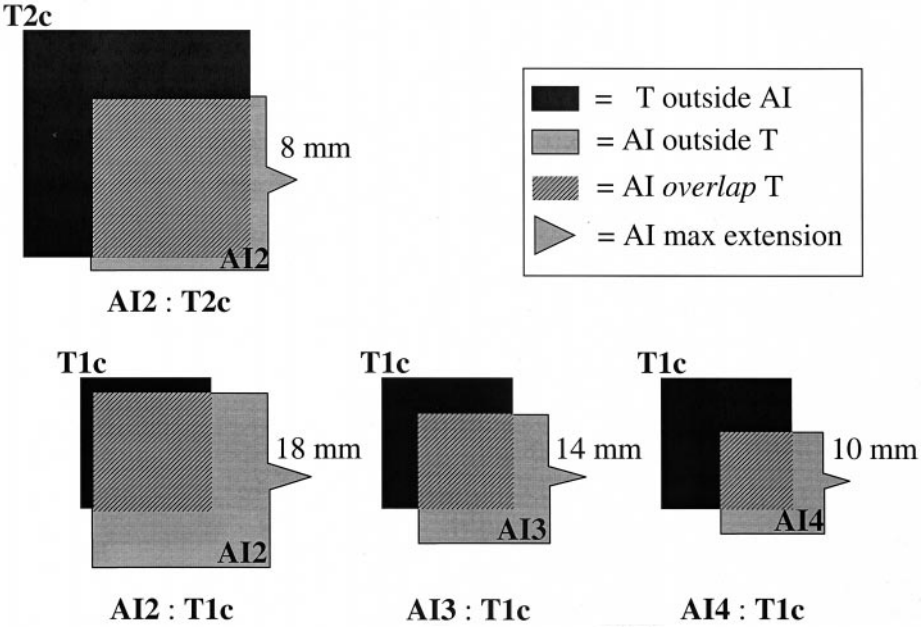

Fig. 9. Graphic summary of results for Grade IV astrocytoma patients. The average relative sizes of the total volumes, the conjoint and disjoint volumes, and the maximum extension of the abnormality index (AI) volume beyond the T volume are displayed.

mm. This implies that the region of T2 hyperintensity does not include all areas of tumor. In addition, the MRI suggested a lesser extent, and a different location, of gross disease, as defined by T1, than did MRSI, as defined by either AI2, AI3, or AI4 levels (Table 3).

A reasonable approach to treatment planning might be to create a plan that simultaneously delivers a conventional dose to the CTV and a higher dose to the GTV. Such an "integrated boost" can be delivered using IMRT. If MRSI data were incorporated into the T1 defined GTV volume for grade III patients, this volume (T1 + [AI outside of T1]) would increase by an average of approximately 500%, 300%, or 150%, depending on the AI contour used. The addition of MRSI AI2 data to MRI T2 data in the definition of the CTV (T2 + [AI2 outside of T2]) would increase the volume only by an additional 15%. In contrast, if the MRSI AI2 were used solely to define the CTV, the volume of the CTV would decrease by approximately 20% compared to the use of T2 alone.

For Grade IV patients, there would be similar, but lesser, effects. The addition of MRSI data to the T1 data in the definition of the GTV would increase the average volume (T1 + [AI outside of T1]) by approximately 150%, 60%, or 50% for AI2, AI3, or AI4, respectively. The effect of adding MRSI AI2 data to the T2 data for CTV definition would increase the volume (T2 + [AI2 outside of T2]) by about 10%; if the MRSI AI2 would be used solely to define the CTV, the volume of the CTV would decrease by approximately 40% compared to the use of T2 alone.

It is important to emphasize that these differences varied markedly from patient to patient and that in a given patient, the extension of the AI volume outside the T1c or T2c volumes at each AI level was not uniform. This reinforces the concern over the use of a uniform margin around the T1 or T2 volume when defining treatment volumes. With suspected gross disease, depending on AI level selected, of 39 to 48 and 24 to 27 mm from the T1c border for Grade III and Grade IV tumors, respectively (Table 3), a conventional uniform boost target margin of 5–20 mm would fail to cover all metabolically active disease. This may help explain the high rate of recurrence of malignant gliomas after RT.

This discussion of the effect MRSI might have on treatment-planning volumes is based upon data from a series of presurgical MRSI and MRI studies. As such, it is not directly applicable to the use of radiation therapy in the postsurgical patient, perhaps the most common use of RT in patients with HGG. However, although the quantitative effect may be different, the qualitative effect should be the same. Because it seems likely that a metabolic study such as MRSI might be better able to determine the volume and location of residual tumor post resection than would an anatomic study such as MRI treatment plans incorporating the MRSI data may target more appropriately areas that would benefit from increased dose.

Although it would appear that MRSI may hold great promise as an aid in defining target volumes for intervention in patients with HGG, it is not without its problems and limitations. A relative limitation in the use of MRSI at the current time is related to the size of the region of excitation (PRESS-box). Currently, MRSI studies at our institution are limited to a maximum volume of acquisition of $16 \times 8 \times 8$ or $12 \times 12 \times 8$ cm. This limitation is time dependent: it takes approximately 1 s to acquire the data per voxel. Thus, the MRSI studies used at our institution add 17 min to the MRI procedure, resulting in a total imaging time of around 90 min. As was shown in Table 1, this volume of excitation was not sufficient to cover the entire region suspect for disease in all patients. This is due in part to the PRESS-box being smaller than the region of interest. It is also due to the need to include as much normal tissue as possible in the PRESS-box to represent accurately the metabolic pattern of noninvolved, normal brain tissue. Until the region of excitation can be enlarged to encompass the entire region of interest plus a certain volume of normal brain, while at the same time maintaining spectral quality, the MRSI studies will not be able to define fully the entire target volume. The shape of the PRESS-box also plays an important role in this issue. The PRESS-box currently in use is a cube. Since it is required that the PRESS-box not include regions of subcutaneous lipid (because of their ability to degrade spectral quality), it is at times difficult to position the box so that it covers the tumor and not the skull. A recent development that may reduce or eliminate this limitation is the use of saturation bands (custom-designed radiofrequency pulses that can saturate subcutaneous lipid) that enable us to conform the PRESS-box to the shape of the skull (53). In the future, high-field magnets and improved radiofrequency coils, resulting in better signal detection, will allow further reduction of the voxel size and an improvement in spatial resolution.

Generating the AI contours for the spectral data involves spatial interpolation. Studies within our department have determined that the contours, as reported here, are accurate to within $\pm$ 2.5 mm (54). This error has to be taken into account when performing a relative volume evaluation, such as was done in this study. Given the AI volumes reported here, introducing this uncertainty into the volume determinations would change them by anywhere from $\pm$ 10–20%. However, because there are also errors in the generation of the T1 and T2 contours, and because all CTVs, be they MRSI or MRI determined, need to be converted to planning target volumes (PTV), this uncertainty can be expected to have a negligible effect on the reported results.

There also may be an effect of edema on the determination of AI volumes. Because the presence of extracellular edema will tend to decrease the density of cells within the edematous region, the magnitude of the spectral signal may be reduced due to a partial volume effect. This would tend to decrease the volume at each AI level. Similarly, areas of necrosis (which may contain some viable, hypoxic cells) admixed with areas of high Cho/NAA ratio could yield lower AI levels. An obvious way to reduce the magnitude of

this issue, as well as the other partial volume effects discussed previously, is to improve the sensitivity of the MRSI.

Another AI level affecting component is the presence of necrosis. Although the qualitative comparison of AI and T1c volumes were the same for Grade III and Grade IV patients, there appeared to be marked differences in the quantitative findings. (Table 4, Fig. 8; Table 5, Fig. 9). A possible explanation for this difference has to do with the finding that the Cho/NAA ratio is lower in Grade IV tumors than in Grade III tumors (23). This is due most likely to the more heterogeneous nature of Grade IV tumors, including small areas of gross necrosis and partial necrosis not identified as regions of hypointensity within the region of T1 contrast enhancement. The presence of these small areas of necrosis will reduce the volume of tumor specific spectral signals at a given AI level designation due to a partial volume effect. Therefore, AI3 and AI4 will not cover as much of T1.

Finally, it is certainly not clear how the AI should be used, if at all, to delineate dose requirements. IMRT allows different doses to be prescribed to different regions of a target. In order for this to be of value, the dose requirements of those regions must be known. Biopsy correlation studies have shown that an AI of 2 is associated with the presence of tumor cells in 100% of cases (24). At first pass, it might be felt that regions with an AI greater than 2 are the ones that should be targeted for an integrated boost, either due to higher metabolic activity per cell or to a greater cell density. However, it also could be argued that it is the regions with a lower metabolic activity that will require a higher dose of radiation. For instance, these regions may have depressed metabolic activity due to poor oxygenation, thus requiring a higher dose to control the cell population.

It is even unclear as to what the AI for a given voxel means in terms of metabolic activity. The voxel may be homogeneous, with all cells having the same AI. It may also be heterogeneous, with areas of very high activity and areas of necrosis. Alternatively, the voxel could contain few cells, each with very high activity, or many cells each with a lower activity. In each case, the AI for the entire voxel would be the same, but the metabolic activity, and, therefore, the dose requirements, of the individual cells making up the voxel may be different.

An in-depth analysis of other MRSI metabolites, such as creatine and lactate, may help differentiate regions of aerobic from regions of anaerobic metabolism, thus detecting hypoxic areas, and higher resolution studies may improve our understanding of what is the metabolic activity in any given region. MRI-based perfusion and diffusion measuring techniques, such as cerebral blood volume (CBV), and apparent diffusion coefficient (ADC) also may allow an indirect determination of where are the oxygen-rich areas. We plan on studying whether some combination of these, or other approaches, may help address the issues of how to relate AI to dose. This will be in conjunction with ongoing studies correlating pre-RT MRSI AI assessment, dose delivered, and post-RT MRSI evidence of tumor control.

The findings reported here also might have significant implications when undertaking surgical intervention. Many current approaches to tumor resection include the use of a frameless surgical treatment planning and navigation system. Before surgery, the surgeon uses a surgical planning system to map out the area to be resected based on the defined target volume as determined from MRI and/or CT studies. The navigation system, used during the resection, allows the surgeon to track the current location of the resection cavity relative to the imaging studies and the treatment plan. As was suggested for RT treatment plans, it can be argued that the use of MRSI might result in a different "planned" volume of resection, and, therefore, a different surgical result.

Obviously, these same factors must be considered when evaluating the results of other focal medical interventions for HGG, such as brachytherapy, hyperthermia, and radiosurgery. Finally, the results of dose-escalation studies, using either external beam or brachytherapy, must be reassessed in light of the fact that incorrect or incomplete volumes may have been targeted for the focal therapy.

CONCLUSION

A recent article by Ling *et al.* emphasizes the "dose painting" and "dose sculpting" that is possible with IMRT, allowing customized dose delivery to various parts of the treatment volume based on their dose requirements (55). To get the most out of this technique, it is a necessary that what needs to be "painted," and how much "paint" is required, be known. The present study shows clearly the discordance in HGG target volumes that result from the use of either anatomic (MRI) or metabolic (MRSI) imaging. This is consistent with the results of other studies comparing PET and SPECT to MRI. Although these studies may help us better understand what needs to be painted, they have not begun to solve the question of how much paint is required.

It is too early to advise the use of biologic imaging as the sole determinant of target volumes. However, the incorporation of metabolic imaging into a treatment planning process that currently relies solely on anatomic imaging seems worthwhile. Much work, using a wide range of new diagnostic techniques, remains to be done to determine how graded levels of metabolic activity can be used to guide the graded levels of dose delivery possible with new treatment techniques such as IMRT. However, it is the belief of the authors that strong consideration should be given to the incorporation of functional imaging into the treatment process for focal treatments or boost techniques for HGG. In addition, the results of controlled dose-escalation trials that used MRI-derived target volumes should be reevaluated given the possibility that these volumes may have been incorrect.

REFERENCES

1. Bleehen NM, Stenning SP. A Medical Research Council trial of two radiotherapy doses in the treatment of grades 3 and 4 astrocytoma. The Medical Research Council Brain Tumour Working Party. *Br J Cancer* 1991;64:769–774.
2. Pirzkall A, Carol MP, Lohr F, *et al*. Comparison of intensity-modulated radiotherapy with conventional conformal radiotherapy for complex-shaped tumors. *Int J Radiat Oncol Biol Phys* 2000;48:1371–1380.
3. Garden AS, Maor MH, Yung WK, *et al*. Outcome and patterns of failure following limited-volume irradiation for malignant astrocytomas. *Radiother Oncol* 1991;20:99–110.
4. Liang BC, Thornton AF Jr, Sandler HM, *et al*. Malignant astrocytomas: focal tumor recurrence after focal external beam radiation therapy. *J Neurosurg* 1991;75:559–563.
5. Wallner KE, Galicich JH, Krol G, *et al*. Patterns of failure following treatment for glioblastoma multiforme and anaplastic astrocytoma. *Int J Radiat Oncol Biol Phys* 1989;16:1405–1409.
6. Nakagawa K, Aoki Y, Fujimaki T, *et al*. High-dose conformal radiotherapy influenced the pattern of failure but did not improve survival in glioblastoma multiforme. *Int J Radiat Oncol Biol Phys* 1998;40:1141–1149.
7. Fitzek MM, Thornton AF, Rabinov JD, *et al*. Accelerated fractionated proton/photon irradiation to 90 cobalt gray equivalent for glioblastoma multiforme: results of a phase II prospective trial. *J Neurosurg* 1999;91:251–260.
8. Frahm J, Bruhn H, Gyngell ML, *et al*. Localized high-resolution proton NMR spectroscopy using stimulated echoes: Initial applications to human brain in vivo. *Magn Reson Med* 1989;9:79–93.
9. Duijn JH, Matson GB, Maudsley AA, *et al*. 3D phase encoding 1H spectroscopic imaging of human brain. *Magn Reson Imaging* 1992;10:315–319.
10. Moonen CT, von Kienlin M, van Zijl PC, *et al*. Comparison of single-shot localization methods (STEAM and PRESS) for in vivo proton NMR spectroscopy. *NMR Biomed* 1989;2:201–208.
11. Arnold DL, Shoubridge EA, Villemure JG, *et al*. Proton and phosphorus magnetic resonance spectroscopy of human astrocytomas in vivo. Preliminary observations on tumor grading. *NMR Biomed* 1990;3:184–189.
12. Barker PB, Glickson JD, Bryan RN. In vivo magnetic resonance spectroscopy of human brain tumors. *Top Magn Reson Imaging* 1993;5:32–45.
13. Moats RA, Watson L, Shonk T, *et al*. Added value of automated clinical proton MR spectroscopy of the brain. *J Comp Assist Tomogr* 1995;19:480–491.
14. Sijens PE, Vecht CJ, Levendag PC, *et al*. Hydrogen magnetic resonance spectroscopy follow-up after radiation therapy of human brain cancer. Unexpected inverse correlation between the changes in tumor choline level and post-gadolinium magnetic resonance imaging contrast. *Invest Radiol* 1995;30:738–744.
15. Negendank WG, Sauter R, Brown TR, *et al*. Proton magnetic resonance spectroscopy in patients with glial tumors: A multicenter study. *J Neurosurg* 1996;84:449–458.
16. Shimizu H, Kumabe T, Tominaga T, *et al*. Noninvasive evaluation of malignancy of brain tumors with proton MR spectroscopy. *AJNR Am J Neuroradiol* 1996;17:737–747.
17. Taylor JS, Langston JW, Reddick WE, *et al*. Clinical value of proton magnetic resonance spectroscopy for differentiating recurrent or residual brain tumor from delayed cerebral necrosis. *Int J Radiat Oncol Biol Phys* 1996;36:1251–1261.
18. Kamada K, Houkin K, Abe H, *et al*. Differentiation of cerebral radiation necrosis from tumor recurrence by proton magnetic resonance spectroscopy. *Neurol Med Chir* 1997;37:250–256.
19. Dowling C, Bollen AW, Noworolski SM, *et al*. Preoperative Proton MR Spectroscopic imaging in brain tumor patients: Correlation with resection specimen histology. *AJNR Am J Neuroradiol* 2001;22:604–612.
20. Graves EE, Nelson SJ, Vigneron DB, *et al*. A preliminary study of the prognostic value of proton magnetic resonance spectroscopic imaging in gamma knife radiosurgery of recurrent malignant gliomas. *Neurosurg* 2000;46:319–328.
21. McDermott MW, Chang SM, Keles GE, *et al*. Gamma Knife radiosurgery for primary brain tumors. In: Germano IM, editor. LINAC and Gamma Knife radiosurgery. ed. Park Ridge: American Association of Neurological Surgeons; 2000. p. 189–202.
22. Nelson SJ. The analysis of volume MRI and MR Spectroscopic Imaging data for the evaluation of patients with brain tumor. *Magn Reson Med* 2000;46:in press.
23. McKnight TR, Noworolski SM, Vigneron DB, *et al*. An automated technique for the quantitative assessment of 3D-MRSI data from patients with glioma. *J Magn Reson Imaging* 2001;13:167–177.
24. McKnight TM, von dem Bussche M, Vigneron DB, *et al*. Correlation of 3D-MRSI Tumor Index with histology in patients with newly diagnosed gliomas (Abstr.). Proceedings of the American Society of Neuroradiology (ASNR) 39th Annual Meeting, Boston, MA, 2001.
25. Lee SW, Fraass BA, Marsh LH, *et al*. Patterns of failure following high-dose 3-D conformal radiotherapy for high-grade astrocytomas: A quantitative dosimetric study. *Int J Radiat Oncol Biol Phys* 1999;43:79–88.
26. Kelly PJ, Daumas-Duport C, Scheithauer BW, *et al*. Stereotactic histologic correlations of computed tomography—and magnetic resonance imaging—defined abnormalities in patients with glial neoplasms. *Mayo Clinic Proceedings* 1987;62:450–459.
27. Matsukado Y, McCarty CS, Kernohan JW. The growth of glioblastoma multiforme (astrocytomas grades 3 and 4) in neurosurgical practice. *J Neurosurg* 1961;18:636–644.
28. Burger PC, Heinz ER, Shibata T, *et al*. Topographic anatomy and CT correlations in the untreated glioblastoma multiforme. *J Neurosurg* 1988;68:698–704.
29. Hochberg FH, Pruitt A. Assumptions in the radiotherapy of glioblastoma. *Neurology* 1980;30:907–911.
30. Oppitz U, Maessen D, Zunterer H, *et al*. 3D-recurrence-patterns of glioblastomas after CT-planned postoperative irradiation. *Radiother Oncol* 1999;53:53–57.
31. Kelly PJ, Daumas-Duport C, Kispert DB, *et al*. Imaging-based stereotaxic serial biopsies in untreated intracranial glial neoplasms. *J Neurosurg* 1987;66:865–874.
32. Halperin EC, Bentel G, Heinz ER, *et al*. Radiation therapy treatment planning in supratentorial glioblastoma multiforme: An analysis based on post mortem topographic anatomy with CT correlations. *Int J Radiat Oncol Biol Phys* 1989;17:1347–1350.
33. Marks JE, Baglan RJ, Prassad SC, *et al*. Cerebral radionecrosis: incidence and risk in relation to dose, time, fractionation and volume. *Int J Radiat Oncol Biol Phys* 1981;7:243–252.
34. Maire JP, Coudin B, Guérin J, *et al*. Neuropsychologic impairment in adults with brain tumors. *Am J Clin Oncol* 1987;10:156–162.
35. Gross MW, Weber WA, Feldmann HJ, *et al*. The value of F-18-fluorodeoxyglucose PET for the 3-D radiation treatment planning of malignant gliomas. *Int J Radiat Oncol Biol Phys* 1998;41:989–995.
36. Grosu AL, Weber W, Feldmann HJ, *et al*. First experience with I-123-alpha-methyl-tyrosine spect in the 3-D radiation

treatment planning of brain gliomas. *Int J Radiat Oncol Biol Phys* 2000;47:517–526.
37. Mosskin M, Ericson K, Hindmarsh T, *et al*. Positron emission tomography compared with magnetic resonance imaging and computed tomography in supratentorial gliomas using multiple stereotactic biopsies as reference. *Acta Radiol* 1989;30: 225–232.
38. Ogawa T, Shishido F, Kanno I, *et al*. Cerebral glioma: evaluation with methionine PET. *Radiology* 1993;186:45–53.
39. Bruhn H, Frahm J, Gyngell ML, *et al*. Noninvasive differentiation of tumors with use of localized H-1 MR spectroscopy in vivo: Initial experience in patients with cerebral tumors. *Radiology* 1989;172:541–548.
40. Preul MC, Caramanos Z, Collins DL, *et al*. Accurate, noninvasive diagnosis of human brain tumors by using proton magnetic resonance spectroscopy. *Nat Med* 1996;2:323–325.
41. Lin A, Bluml S, Mamelak AN. Efficacy of proton magnetic resonance spectroscopy in clinical decision making for patients with suspected malignant brain tumors. *J Neurooncol* 1999;45:69–81.
42. Meyerand ME, Pipas JM, Mamourian A, *et al*. Classification of biopsy-confirmed brain tumors using single-voxel MR spectroscopy. *AJNR Am J Neuroradiol* 1999;20:117–123.
43. Brown TR, Kincaid BM, Ugurbil K. NMR chemical shift imaging in 3 dimensions. *Proc Natl Acad Sci USA* 1982;79: 3523–3526.
44. Segebarth CM, Balériaux DF, Luyten PR, *et al*. Detection of metabolic heterogeneity of human intracranial tumors in vivo by 1H NMR spectroscopic imaging. *Magn Reson Med* 1990; 13:62–76.
45. Fulham MJ, Bizzi A, Dietz MJ, *et al*. Mapping of brain tumor metabolites with proton MR spectroscopic imaging: Clinical relevance. *Radiology* 1992;185:675–686.
46. Noworolski SM, Nelson SJ, Henry RG, *et al*. High spatial resolution 1H-MRSI and segmented MRI of cortical gray matter and subcortical white matter in three regions of the human brain. *Magn Reson Med* 1999;41:21–29.
47. Luyten PR, Marien AJ, Heindel W, *et al*. Metabolic imaging of patients with intracranial tumors: H-1 MR spectroscopic imaging and PET. *Radiology* 1990;176:791–799.
48. Michaelis T, Merboldt KD, Bruhn H, *et al*. Absolute concentrations of metabolites in the adult human brain in vivo: Quantification of localized proton MR spectra. *Radiology* 1993;187:219–227.
49. Rango M, Spagnoli D, Tomei G, *et al*. Central nervous system trans-synaptic effects of acute axonal injury: A 1H magnetic resonance spectroscopy study. *Magn Reson Med* 1995;33: 595–600.
50. Poptani H, Gupta RK, Roy R, *et al*. Characterization of intracranial mass lesions with in vivo proton MR spectroscopy. *AJNR Am J Neuroradiol* 1995;16:1593–1603.
51. Nelson SJ, Huhn S, Vigneron DB, *et al*. Volume MRI, and MRSI techniques for the quantitation of treatment response in brain tumors. Presentation of a detailed case study. *J Magn Reson Imaging* 1997;7:1146–1152.
52. Wald LL, Nelson SJ, Day MR, *et al*. Serial proton magnetic resonance spectroscopy imaging of glioblastoma multiforme after brachytherapy. *J Neurosurg* 1997;87:525–534.
53. Tran TK, Vigneron DB, Sailasuta N, *et al*. Very selective suppression pulses for clinical MRSI studies of brain and prostate cancer. *Magn Reson Med* 2000;43:23–33.
54. Graves EE, Pirzkall A, Nelson SJ, *et al*. Incorporation of 1H Magnetic Resonance Spectroscopic Imaging Data in the Radiation Treatment Planning Process (Abstr.). Proceedings of the International Society of Magnetic Resonance in Medicine (ISMRM) 8th Annual Meeting, Glasgow, UK, 2001; p. 2305.
55. Ling CC, Humm J, Larson S, *et al*. Towards multidimensional radiotherapy (MD-CRT): biological imaging and biological conformality. *Int J Radiat Oncol Biol Phys* 2000;47:551–560.